

Article

# Fatigue Reliability Analysis of Rib-To-Deck Joints Using Test Data and In-Situ Measurements

Kaifeng Zheng, Xiaoyang Feng, Junlin Heng \*, Jin Zhu and Yu Zhang

Department of Bridge Engineering, School of Civil Engineering, Southwest Jiaotong University, Chengdu 610031, China; kfzheng@swjtu.edu.cn (K.Z.); fxy505@foxmail.com (X.F.); zhujin@swjtu.edu.cn (J.Z.); zhangyu2006@my.swjtu.edu.cn (Y.Z.)

\* Correspondence: j.l.heng@my.swjtu.edu.cn; Tel.: +86-182-8017-6652

Received: 24 October 2019; Accepted: 7 November 2019; Published: 11 November 2019



**Abstract:** In this paper, the fatigue performance of rib-to-deck joints in orthotropic steel decks (OSDs) using thickened edge U-ribs (TEUs) and the OSD using conventional U-ribs (CUs) are investigated based on the fatigue test result and in-situ monitoring data. Firstly, comparative fatigue tests were carried out with full-scale rib-to-deck specimens. Probability–stress–life (P–S–N) curves were derived through the test data measured from a total of 18 specimens, including 7 CU specimens and 11 TEU specimens. According to the results, the TEU can lead to a notable enhancement in the fatigue strength of rib-to-deck joints, i.e., 21.4% in terms of nominal stress and 21.1% in terms of hot spot stress. After that, a typical OSD steel bridge was selected as the prototype to investigate the fatigue performance of rib-to-decks in the OSD using TEUs under actual applications. In the analysis, the uncertainty in both fatigue strength, and vehicle loads were considered. A multi-scale finite element model of the prototype bridge was established, and numerical analysis conducted to derive the vehicle-induced stress spectra of the rib-to-deck joints in critical positions. In the derivation, a stochastic traffic model was employed, through which the in-situ measurement was incorporated. Finally, fatigue reliability analysis was carried out for the prototype bridge based on the above works. The result showed that a notably higher fatigue reliability can be expected in the rib-to-deck joint in OSDs using TEUs when compared with the joints in OSDs using CUs, which in turn can lead to notable improvement in fatigue life. For instance, under the target reliability of 2.3, the fatigue life of the two critical rib-to-deck joints were, respectively, increased by 153% and 155% when using TEUs.

**Keywords:** orthotropic steel deck; thickened edge U-ribs; flux cored arc welding; fatigue test; in-situ measurement; fatigue reliability

## 1. Introduction

The orthotropic steel deck (OSD) has been widely employed in steel bridges, along with the evolution more than half a century after it was first invented as a battle deck in the 1930s. Compared with other types of decks, the structural members in OSDs are highly integrated, leading to superiorities such as large loading-capacity, speedy construction, and light self-weight [1]. During fabrication, a considerable amount of welding works is applied to make up the complicated structural details in OSDs. As a result, fatigue cracking of welded joints becomes a very prominent issue in OSDs, especially when the truck traffic volume is high [2,3]. Among the different types of welded joints, fatigue cracks are frequently observed in the rib-to-deck (RD) joint located between the U-rib and deck plate [4]. Two major factors can account for the phenomenon—the large amount of RD joints and the vehicle loads directly applied on the joints. As a result, cracking in RD joints will cause serious consequences, i.e., the damage to the pavement and even the failure of the deck system.

Obviously, the cracking issue will hinder the OSD from the continuous service over a design life of 100 years [5].

Generally, two types of fatigue failure are frequently observed in RD joints, i.e., the weld root-to-deck cracking and the weld toe-to-deck cracking. In the case of weld root-to-deck cracking, the fatigue crack first initiates at the weld root on the deck side and then propagates into the deck plate. This type of cracking is often observed in the early-built OSD bridges, especially those erected in the 1990s and early 2000s. According to the studies [1,6], the root cracking is mainly controlled by the penetration depth of U-ribs and the fit-up gap between the deck plate and U-rib before welding. When the fit-up gap is well controlled under 0.5 mm during the fabrication, root cracking can be prevented [7,8]. Thus, the weld toe-to-deck cracking is now of particular concern, in which the crack initiates at the deck toe and then propagates into the deck plate.

In recent years, extensive research efforts have been performed to solve the fatigue issue of RD joints, including the post weld treatment and innovations of structural details. The post weld treatment can be classified by the target of improvement, i.e., the weld profile and residual stress [9]. In terms of the weld profile, the grinding and TIG-dressing can be employed to generate a smooth transition between the weld and the base metal at the weld toe. As a result, the stress concentration can be ameliorated at the weld toe, which can in turn lead to the improvement in the fatigue strength. Another type of treatment is to improve the residual stress condition through peening methods, including hammer-peening, needle-peening, brush-peening and the ultrasonic impact treatment (UIT). As suggested by Haagensen and Maddox [9], the above treatments can result in a significant enhancement in the fatigue strength. For structural steel with yield strengths less than 355 MPa, which is commonly used in steel bridges, the fatigue strength of the treated joint can be improved by 30% when compared with the as-welded joint. It is also worth stating that the application of post weld treatments is not against the application of novel structural details. As a result, further improvement can be expected in the fatigue strength of rib-to-deck joints.

In the case of detail innovation, there are three representative novel technologies, including the thickened edge U-rib (TEU) [10], both-side fillet welding [11], and steel–concrete composite deck [12]. The concept of TEUs is to increase the thickness of rib walls at the edge through the continuous rolling method, as shown in Figure 1. The fabrication and labor costs will be just slightly increased in TEUs, since a standardized steel sheet is used with the special operation on the edge only. At the same time, the thickness available for welding in rib walls can be notably improved with the thickened edge. Taking the 8 mm-thick U-rib as an example, which is commonly used in OSDs, the edge thickness can be increased from 8 to 12 mm (i.e., 50%) when using TEUs. Besides, a smooth transition is generated at the edge of TEUs during the rolling process, as shown in Figure 1b. As a result, no further work is required to create a bevel for welding, and the stress concentration could also be ameliorated in the RD joint. As shown in Figure 1b, the U-rib is in closed shape, making it very difficult to perform welding works from the inside. Thus, the single-side welding is usually utilized to perform welding from the outside of U-ribs, with a desired penetration rate around 75% to 80% to avoid the negative effect of melt-through [1,13,14].

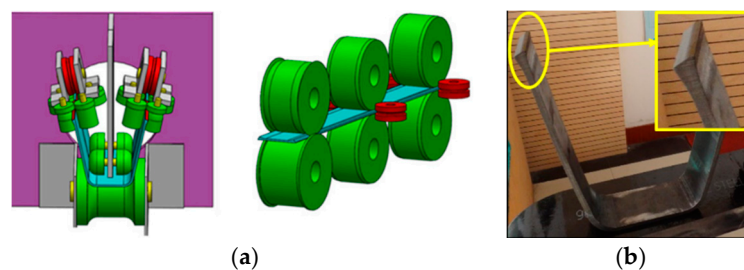


**Figure 1.** Illustration of thickened edge U-ribs: (a) fabrication process and (b) view.

In the both-side fillet welding technology, the rib wall is welded to the deck plate from both the inside and outside, with the application of a small inner welding machine customized for RD joints only. Intuitively, the fatigue strength of RD joints can be enhanced by the both-side welding since the integrity is improved. However, fatigue test data are still required to prove the effectiveness and feasibility of the both-side welding since little data are currently available. Besides, an additional fatigue-critical point is introduced by the both-side welding, i.e., since an inner weld toe will be formed inside the U-rib [11]. As a result, some negative effects may be imposed on the fatigue strength and is due to be verified by fatigue tests. Unlike the above two methods, in which the target is to improve the fatigue strength directly, the composite deck technology tries to reduce the vehicle-induced stress ranges in RD joints by introducing a layer of ultra-high-performance concrete (UHPC) [15] above the deck surface. The UHPC layer is connected to the deck plate by shear keys, usually shear studs, through which the layer can work together with the deck against the external loads [16]. According to the test data [17], the stress ranges can be significantly reduced in RD joints in composite decks, i.e., about almost 80 percent. However, a new fatigue-critical detail was also found in the composite deck, i.e., the welded joint between the studs and the deck plate. The stud-to-deck joint is found to be highly prone to fatigue failure due to the high-level stress range induced by the applied cyclic loads. After the cracking of studs, the stress range in RD joints would increase to almost the same level as the joint in traditional decks without the UHPC layer. When the loading was continued, a very similar failure model was observed in RD joints due to the rebounded stress ranges.

Based on the above analysis, the application of TEUs seems to be both applicable and promising in enhancing the fatigue performance of RD joints. A series of studies was performed on the fatigue strength of RD joints using TEUs through the fatigue tests on full-scale rib-to-deck specimens [10,18]. According to the test data of 11 specimens, the weld toe-to-deck cracking pattern is observed. The result also suggests that the application of TEUs can notably enhance the fatigue strength of RD joints. Besides, a further experimental study was carried out on two full-scale OSD segment specimens, including one using conventional U-ribs (CUs) and one using TEUs [19]. A similar fatigue failure model of toe-to-deck cracking was observed in both the two specimens, while the fatigue life of rib-to-decks in the CU specimen and the TEU specimen were 4.19 and 8.59 million cycles, respectively. Based on the above fatigue test, the effectiveness of TEUs was proved in enhancing the fatigue performance of rib-to-deck joints. However, due to the limitation in the number of tested specimens, a practical probability–stress–life (P–S–N) curve has yet to be established through statistics analysis on a sufficient set of test data.

Another essential work about the TEU is to validate its effectiveness in actual engineering projects. Apart from the fatigue strength, the vehicle-induced stress ranges are of the same importance in determining fatigue performance. In most codes of practice [20–22], the stress ranges are represented by an equivalent stress range solved by the deterministic analysis with standard fatigue truck models. Obviously, this type of method is simple and straightforward, but it may cause notable errors in fatigue life prediction since the random feature of fatigue is not explicitly considered [23]. Alternatively, reliability analysis can be applied to predict the fatigue life of welded joints under an assumed target reliability [24], with the consideration of uncertainties in both fatigue strength and action. At the same time, with the rapid improvement in structural health monitoring (SHM) [25], the measurement-based structural analysis gradually becomes available and applicable. For instance, in [26], in-situ monitoring data were utilized to predict the fatigue life of bridge suspenders through reliability analysis. With respect to TEUs, numerical evaluations have been previously conducted on the fatigue performance of rib-to-deck joints in OSDs using TEUs and the joints in OSDs using CUs [27]. The result suggested that the fatigue life of RD joints can be prolonged by 141% to 161% when using TEUs. In the numerical study, the fatigue strength of RD joints was determined after the existing S–N curves and some preliminary results obtained from the limited test data. However, it is worth noting that the numerical fatigue evaluation was performed in a deterministic way to some degree, even if the stress spectra of RD joints were derived based on a stochastic traffic model.

The aim of the present study was to evaluate the fatigue performance of rib-to-deck (RD) joints in orthotropic steel decks (OSDs) using TEUs under a reliability-based framework incorporating test data and in-situ measurements. Based on the preliminary experimental studies of 11 full-scale specimens in [10,18], a series of fatigue tests was first carried out with a total of 7 full-scale specimens. Through the test data of the above 18 specimens, probability–stress–life (P–S–N) curves were established for RD joints through statistical analysis. Meanwhile, a typical OSD bridge was selected as the prototype and the traffic data from in-situ measurements were considered. On this end, a novel reliability-based evaluation approach was proposed to incorporate the fatigue test result and in-situ measurement data. In the approach, numerous studies have been employed to establish the stress spectra of RD joints from the traffic data through large-scale sampling. Based on the proposed approach, fatigue reliability analysis was performed for the RD joint in OSDs using TEUs and the one in OSDs using CUs. With the assumed target reliability, the fatigue life of RD joints in the above two deck systems were predicted and compared, indicating the superiority of TEUs over CUs in OSDs.

## 2. Fatigue Tests of Rib-To-Deck Joints

### 2.1. Design of Specimens

As widely acknowledged, the fatigue test is the most reliable and somehow inevitable approach in the study on fatigue performance of OSDs [28]. Since extensively welded joints are used in OSDs, various types of fatigue-critical details existed [29], including the rib-to-deck joint, the rib-to-floor beam joint, and the floor beam-to-deck joint. Meanwhile, the structural behavior of OSDs is extremely complicated, because of the large number of the details in OSDs and the high integrity among the details [29]. To this end, several types of fatigue cracking may occur in the fatigue test when the segment model is employed [30]. In order to focus on the fatigue performance of RD joints, which is the main target of this study, rib-to-deck specimens are used in the fatigue test. A total of 7 specimens are fabricated using Q345qD steel [31] (similar to the British steel grade S355NL), including 2 CU specimens and 5 TEU specimens. The specimen consists of a 16 mm-thick deck and an 8 mm-thick U-rib, which are connected by two RD joints, as shown in Figure 2a. The RD joint in CU specimens and the joint in TEU specimens are illustrated in detail in Figure 2b. It is worth stating that the width of the U-ribs is measured at the mid-plane of the rib wall, which is the same in the two types of U-ribs. In the fabrication, 2 mm of the rib wall is not welded to avoid the negative effect of weld melt-through on fatigue strength. Under this design, the penetrated thickness of rib walls in TEU specimens is increased from 6 to 10 mm, i.e., an increment of almost 67%. At the same time, the weld leg length on the deck plate is also notably increased (from 11 to 15 mm). During the welding works, a semi-auto welding machine was employed, and the welding parameters were kept the same as in the preliminary tests [18,19]. The welds have been made by the flux cored arc welding (FCAW) protected with CO<sub>2</sub>, and the rate of shielding gas flow is 20 L/min. The designation of the welding wire is E501T-1(E71T-1C) [32,33], with the diameter of 1.2 mm. Correspondingly, and the contact tip to work distance (CTWD) is determined as 15 times the diameter, i.e., 18 mm. The arc voltage and welding current are, respectively,  $31 \pm 2$  V and  $290 \pm 20$  A, with a travel speed of  $380 \pm 20$  mm/min.

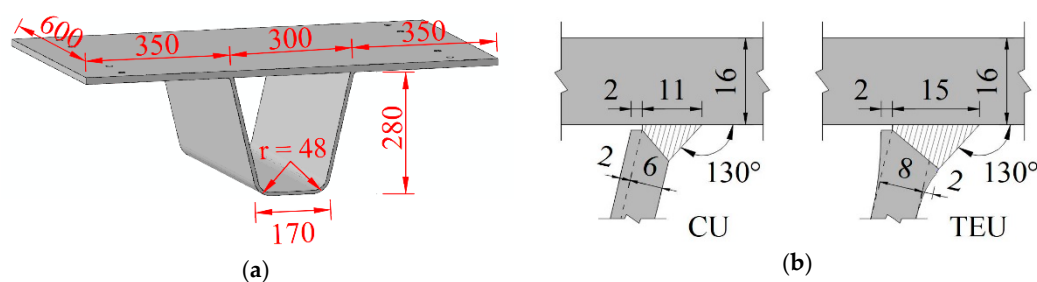


**Figure 2.** Schematic view of rib-to-deck specimens: (a) overview and (b) rib-to-deck joints.

### 2.2. Test Setup

The specimen is simply supported on a testing platform, with the actuator on the longitudinal center of the left joint, as shown in Figure 3a,b. In order to distribute the applied load and reacting force, rubber plates are installed between the loading actuator, specimen and supporting platform. Besides, a pressure-sensitive film is installed between the specimen and actuator, as shown in Figure 3b, to verify the uniformity of loading distribution. A coordinate system is introduced to illustrate the position of the actuator, shown in Figure 3a, with the origin at the left-front corner of the deck. Under the system, the coordinate of the center of the actuator is (455 mm, 300 mm).

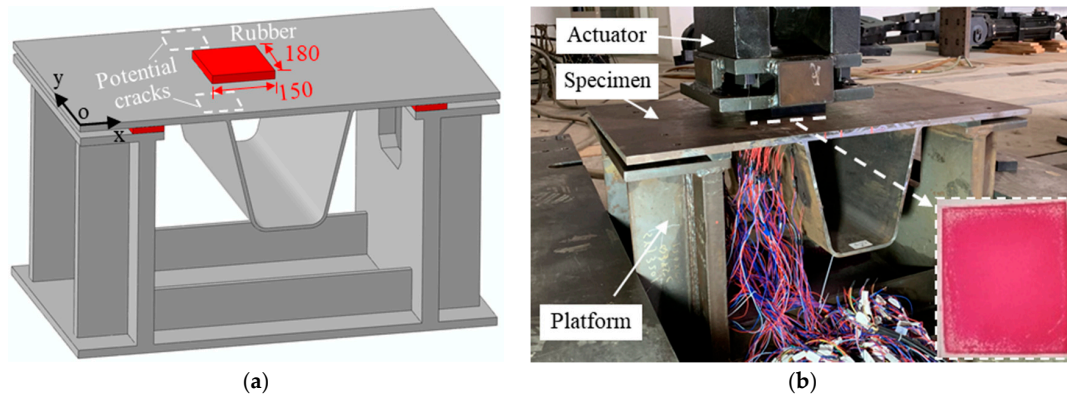


Figure 3. Test setup: (a) schematic view and (b) photography.

The specimens were cyclically loaded with the constant amplitude loads, using the hydraulic test device MTS system [34]. The loading frequency was set as 3.25 Hz, which is acceptable for the fatigue test of large civil structures. Various levels of cyclic loads were applied on the different specimens, to obtain stress–life (S–N) data under a wide range of stress levels. Meanwhile, the ratio of the maximum to the minimum loads was kept the same as the value in the previous test [18,19], i.e., 3.0. Table 1 summarizes the cyclic loads applied on each specimen.

Table 1. Cyclic loads applied on each specimen (kN).

CODE	Maximum Load	Minimum Load	Range of Loads
CU6	15	50	35
CU7	15	50	35
TEU7	15	50	35
TEU8	18	60	42
TEU9	19	65	46
TEU10	19	65	46
TEU11	22	74	52

According to the test result of similar specimens in [10], fatigue cracking is highly expected to initiate at the deck-side weld toe at two potential cracking sites shown in Figure 3a. Based on this assumption, the stress gauge was set with special emphasis on the weld toe at the deck side, as shown in Figure 4.

Both the nominal stress and hot spot stress were considered in the measurement. The hot spot stress is calculated by the extrapolation with the “0515” rule suggested by IIW [35], as shown in Equation (1).

$$\sigma_{hs} = 1.5\sigma_{0.5t} - 0.5\sigma_{1.5t} \tag{1}$$

where  $t$  stands for the thickness of the plate under consideration, i.e., the deck plate in this study;  $\sigma_{hs}$  is the hot spot stress;  $\sigma_{0.5t}$  and  $\sigma_{1.5t}$  are, respectively, the stress measured at the distance of 0.5 and 1.5  $t$  away from the deck toe, i.e., D8-X and D24-X in this study.



As per the rule, two reference points are used in calculating the hot spot stress, whose distances to the weld toe are 8 mm (named as D8-1 to D8-16) and 24 mm (named as D24-1 to D24-16), respectively. Since the cracking in the RD joint would result in strain drops in nearby gauges, the dynamic strain monitored during loading could be utilized to reflect the development of fatigue cracks [18]. Thus, additional dynamic gauges are deployed, which are named as D-1 to D-21. Due to the difference in the weld leg length between the CU specimen and TEU specimen, the distance between the strain gauges and loading point will be different. Since the mid-plane width of the two types of U-ribs is the same, it can be calculated from Figure 2b that the distance from the weld toe to the loading point in TEU specimens is 2 mm longer than that in CU specimens. Meanwhile, it can be determined from Figures 1 and 3 and the coordinate of the loading point that the distance from the weld toe to the loading point is 119 and 121 mm in the CU and TEU specimens, respectively. For the first-row reference gauges, which are 8 mm away from the weld toe, the distance between the loading point and gauges is, respectively, 127 mm and 129 mm in the two types of specimens, i.e., a difference of less than 1.6%. In the case of the second-row reference gauges, which are 24 mm away from the weld toe, the difference is no more than 1.4%. Based on the above analysis, the distance between the strain gauges and the loading point can be assumed to be the same in the two types of specimens. Besides, penetrant testing (PT) checks were also performed to identify the cracking of RD joints during the test. At first, the PT check is conducted after every 50,000 cycles. After any fatigue crack is observed, the interval of PT checks is narrowed to every 10,000 cycles.

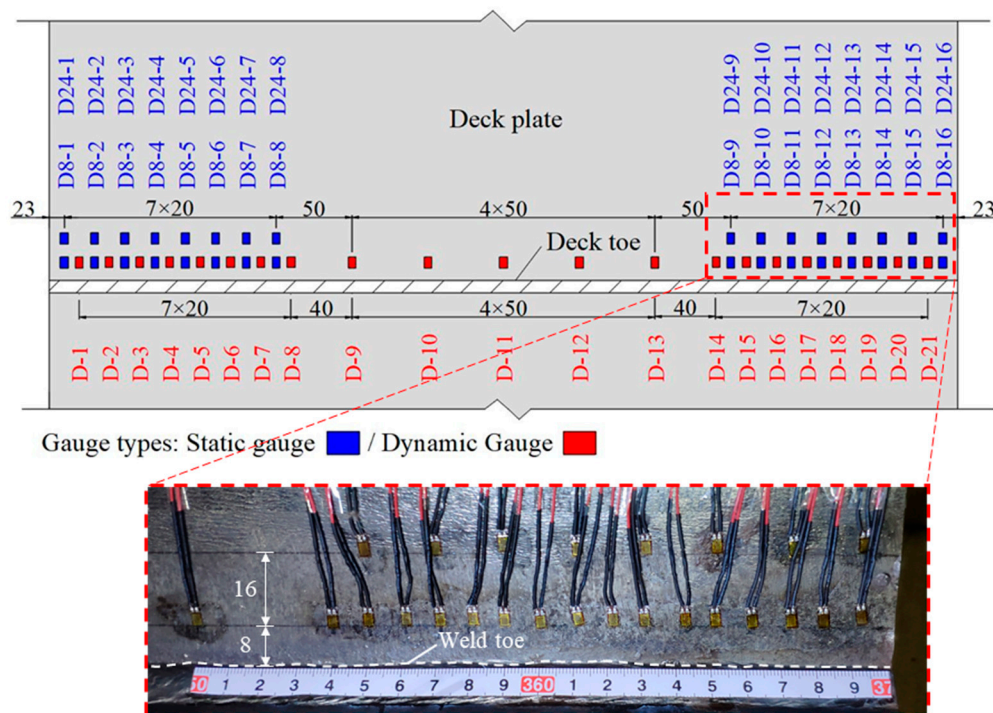


Figure 4. Strain gauges installed on specimens.

### 2.3. Test Result

In all the tested specimens, the fatigue crack first initiates at the weld toe on the deck side, and then propagates along both the thickness and length of the deck plate, as shown in Figure 5. In the test, the failure of specimens is assumed when the fatigue crack penetrates through the thickness of the deck plate. After that, the test will be terminated, and the number of the loading cycles applied is taken as the fatigue life.

As aforementioned, dynamic gauges have been applied to monitor strain drops near the crack, which can in turn reflect the development of fatigue cracks during loading. Figure 6 shows the strain drops in the dynamic gauges installed on specimen TEU-10.

The result indicated that two fatigue cracks were initiated at the two deck toes which were about 70 to 80 mm away from the center of actuator. With the increase in loading cycles, the two cracks propagated along both the depth and length of the deck plate. It can be found that the cracking pattern measured by the gauges is highly consistent with the visual observation. At the same time, the strain drops at the two crack-initiate sites, i.e., D-4 and D-18, are illustrated in detail in Figure 7. The strain drops of 10% can be observed after about  $1.2 \times 10^6$  cycles in D-4 and  $1.43 \times 10^6$  cycles in D-18, respectively. After that, the strain gradually drops with the loading cycles, from almost 170 MPa to about 30 MPa. It is interesting to note that, the strain drops in D-18 a bit later than in D-4. However, the value in D-18 meet that in D-4 after  $1.55 \times 10^6$  cycles and then surpasses, since the slope of strain drops is increasing in D-18 while almost unchanged in D-4.

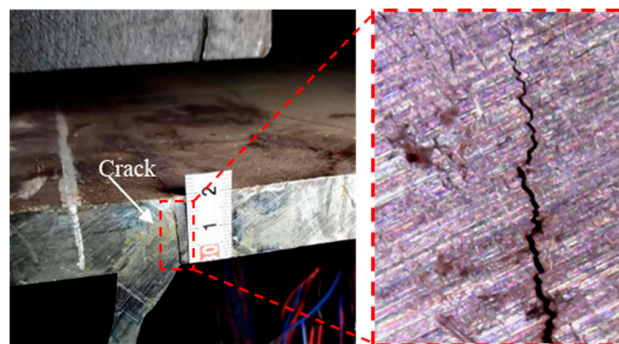


Figure 5. Typical fatigue cracking pattern of tested specimens.

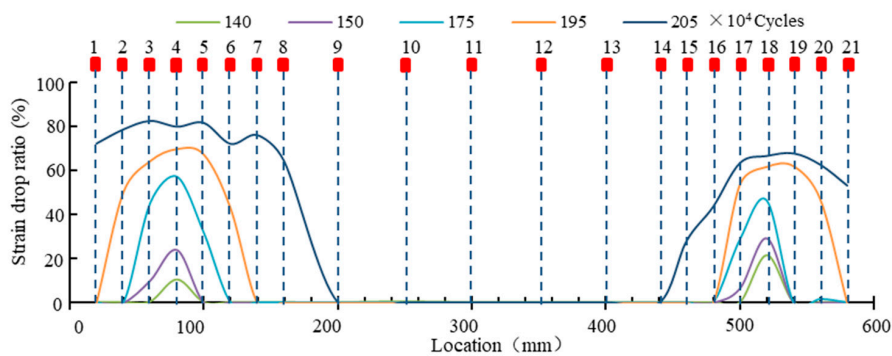


Figure 6. Strain drops measured in TEU-10.

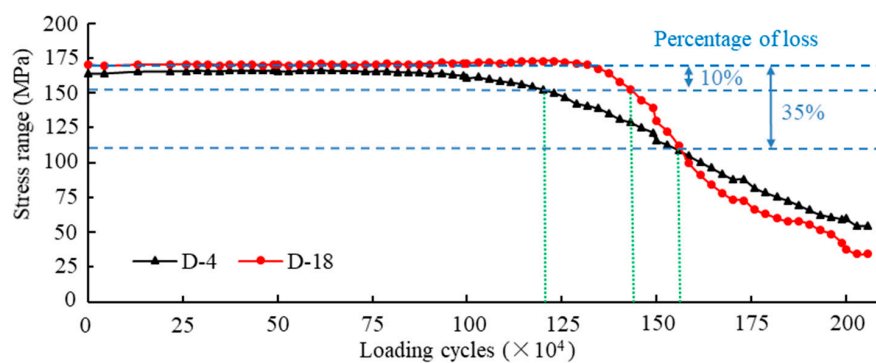


Figure 7. Stress ranges measured at the two crack-initiate sites in TEU-10.

In the tests, different cyclic loads have been applied on the different specimens. For comparison purposes, the measured stress–life data have been unified to the equivalent fatigue strength under the same equivalent fatigue life [36], as shown in Equation (2).

$$\Delta\sigma_{eqv} = \left(\frac{N_{test}}{N_{eqv}}\right)^{\frac{1}{m}} \cdot \Delta\sigma_{test} \tag{2}$$

where  $\Delta\sigma_{eqv}$  stands for the equivalent fatigue;  $\Delta\sigma_{test}$  and  $N_{test}$  are the measured stress range and corresponding failure cycles;  $N_{eqv}$  is the equivalent fatigue life, set as  $2 \times 10^6$  cycles in this study;  $m$  is the material-related power index, assumed to be 3 as a common practice.

Based on the above analysis, the stress–life data are summarized in Table 2, accompanied by the data of 11 specimens previously tested [10,18].

**Table 2.** Stress–life data measured from fatigue tests.

CODE	Measured Stress Range (MPa)		Failure Cycles ( $\times 10^4$ )	Equivalent Fatigue Strength (MPa)		Average Equivalent Fatigue Strength (MPa)	
	Nominal	Hot Spot		Nominal	Hot Spot	Nominal	Hot Spot
CU1 *	81	98	269	89	108		
CU2 *	103	121	255	112	131		
CU3 *	123	149	91	95	115		
CU4 *	58	81	824	93	130	103	
CU5 *	81	113	314	94	131	(13.0) <sup>1</sup>	128
CU6	115	135	206	116	136		
CU7	111	132	263	121	145		
TEU1 *	114	144	147	103	130		
TEU2 *	119	146	162	111	136		
TEU3 *	125	154	234	132	162		
TEU4 *	129	153	193	127	151		
TEU5 *	78	113	648	115	167		
TEU6 *	106	131	223	110	136	125	
TEU7	114	144	333	135	171	(14.1)	155
TEU8	139	160	204	140	161		
TEU9	151	187	129	130	162		
TEU10	147	170	210	149	173		
TEU11	174	211	75	125	152		

\*: The specimen previously tested in [10,18]. <sup>1</sup> The value in brackets is the standard deviation.

The test result suggests that the fatigue strength is relatively higher in the TEU specimens than in the CU specimens, indicating the effectiveness of TEUs in enhancing the fatigue performance of rib-to-deck joints. In terms of nominal stress, the average value of equivalent fatigue strength is 125 MPa in TEU specimens, i.e., 21.4% higher than the strength of 103 MPa in the CU specimens. In the case of hot spot stress, the average strength of TEU specimens and CU specimens is respectively 155 and 128 MPa, i.e., an enhancement of 21.1%. Meanwhile, it is also worth noting that the standard deviation of the two types of specimens are similar, which is slightly higher in TEU specimens. Due to the random nature in fatigue strength, the higher deviation can be attributed to the larger number of the tested TEU specimens.

### 3. Derivation of Probability–Stress–Life Curves

#### 3.1. Statistics Method for P–S–N Derivation

Based on the above analysis, the fatigue strength of TEU specimens and CU specimens are compared in terms of the mean value. However, in the fatigue design, it is risked and unreasonable to directly use the mean value, which stands for a failure rate of 50%. Instead, the stress–life curve established under a specific survival probability is generally applied, which is also called as the probability–stress–life (P–S–N) curve. To derive the P–S–N curve, the uncertainties in fatigue strength should be fully considered through the statistics analysis on the test data.

In the fatigue design, Wohler’s equation is generally applied as the basic model for the stress–life relation [36], as shown in Equation (3) (power form) and Equation (4) (log–log form).

$$\Delta\sigma^m \times N = C \tag{3}$$



$$m \times \log \Delta\sigma + \log N = \log C \tag{4}$$

where  $\Delta\sigma$  stands for the applied stress range;  $N$  is the fatigue life;  $m$  and  $C$  are the material-related power index and constant, respectively.

For welded joints in steel structures, the power index  $m$  can be treat as a fixed value of 3 while the constant  $C$  accounts for the uncertainty in fatigue strength [35]. On this end, the P–S–N can be established based on the characteristic value of the constant  $C$ , or more generally its logarithm  $\log C$ , under a specific survival rate. In serval codes of practice [20,21], the value  $\log C$  is assumed to be normal distributed and a survival probability of 97.7% is considered. As a result, the characteristic value of  $\log C$  can be calculated as the sample mean value minus two times the sample deviation.

Obviously, the 97.7% survival rate-based method is straightforward and easy to use. However, the uncertainty in the estimators, i.e., the sample and deviation, is totally ignored in the above method, which may cause errors and even risks in the fatigue design. One this end, the statistics approach proposed by IIW [36] is also considered, in which the uncertainty in estimators is included using the tolerant interval, as shown in Equations (5) and (6).

$$x_c(\log C) = x_m(\log C) - k \cdot Std(\log C) \tag{5}$$

$$k = t_{p,n-1} / \sqrt{n} + \Phi_\alpha^{-1} \cdot \sqrt{(n-1) / \chi_{(1+\beta)/2,n-1}^2} \tag{6}$$

where  $x_c$  is the characteristic value;  $x_m$  and  $Std$  stand for the sample mean and deviation, respectively;  $n$  is the number of tested specimens;  $t_{p,n-1}$  is the critical value of t-distribution with  $n - 1$  degrees at the confidence level  $p$ ;  $\Phi_\alpha^{-1}$  is critical value of standard normal distribution at the survival rate  $\alpha$ ;  $\chi_{(1+\beta)/2,n-1}^2$  is the critical value of chi-square distribution with  $n - 1$  degree at the confidence level  $(1 + \beta)/2$ .

As per the suggestion by IIW [36], the survival rate  $\alpha = 95\%$  can be applied with the confidence levels  $p = \beta = 75\%$  in deriving the characteristic value of  $\log C$ . It can be also found that the IIW method takes into consideration the influence of the number of specimens on fatigue strength, through incorporating the uncertainty in estimators.

### 3.2. Result and Discussion

The P–S–N curves of rib-to-deck joints were first derived using the traditional assumption with the 97.7% survival rate, in which the uncertainty in estimators was not considered. The result of the two types of specimens is shown in Figure 8a,b, in terms of nominal stress and hot spot stress, respectively.

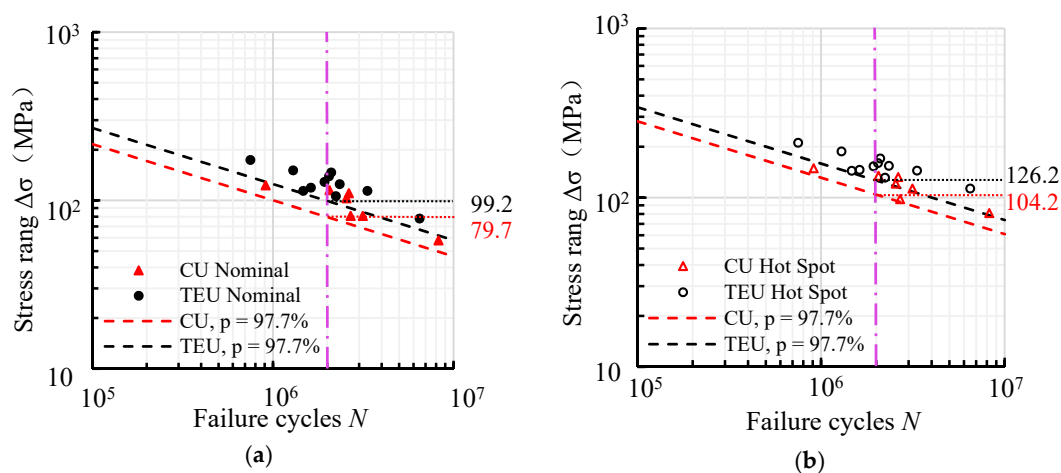


Figure 8. P–S–N curve under the survival rate of 97.7%: (a) nominal stress and (b) hot spot stress.

Generally, the characteristic fatigue strength at 2 million cycles, called the “FAT” value, can be utilized to category the class of fatigue-critical details [20,22]. Based on the above analysis, the FAT value of the CU specimens was 79.7 MPa in terms of nominal stress and 104.2 MPa in terms of hot spot stress. It is interesting to note that the derived curve is slightly higher than the curve proposed in Eurocode 3 [20], i.e., the FAT 70 curve in nominal stress and the FAT 100 curve in hot spot stress. However, the improvement in welding technology can account for the difference since the curve in Eurocode 3 is based mainly on fatigue test data obtained before the 1980s. For the TEU specimens, the FAT values were 99.2 and 126.2 MPa in terms of nominal stress and hot spot stress, respectively. Compared with CU specimens, the FAT value in TEU specimens increased by 24.5% in nominal stress and 21.1% in hot spot stress, further indicating the effectiveness of TEUs in enhancing the fatigue strength of rib-to-deck joints.

At the same time, the IIW method was also applied to derive the P–S–N curve of rib-to-deck joints, under the survival rate of 95% and tolerant limit of the 75% for the estimators. The derived curves are shown in Figure 9.

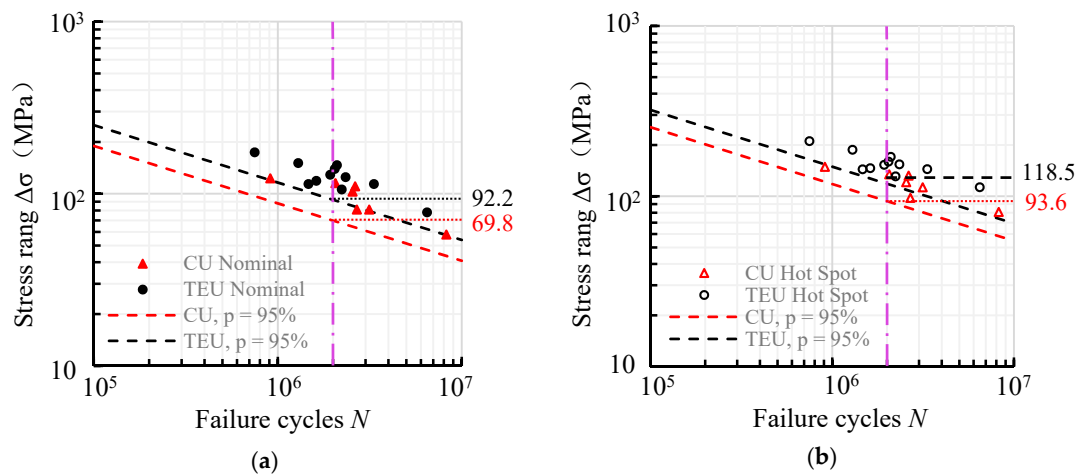


Figure 9. P–S–N curve under the survival rate of 95%: (a) nominal stress and (b) hot spot stress.

Compared with the CU specimens, the FAT value in the TEU specimens were 34.1% and 28.5% higher in terms of nominal stress and hot spot stress, respectively. It is worth noting that the FAT values in Figure 9 are notably lower than that in Figure 8, even if the survival rate is reduced from 97.7% to 95%. The comparison between Figures 8 and 9 suggests that a more conservative P–S–N curve can be obtained by the IIW method, since the uncertainty in estimators is considered. To this end, it is suggested that the IIW method-based P–S–N curves in the fatigue design of rib-to-deck joints be used. After rounded off with engineering experience, for rib-to-deck joints in OSDs using TEUs, the FAT 90 and FAT 115 curves are proposed in terms of nominal stress and hot spot stress, respectively. Meanwhile, for the joints in OSDs using CUs, the FAT 70 curve is proposed under the nominal stress and while the FAT 90 curve is suggested when using the hot spot stress approach.

#### 4. In-Situ Measurement-Based Fatigue Reliability Analysis

##### 4.1. Analysis Method of Fatigue Reliability

In the reliability analysis, the major task is to solve the possibility that the resistance is lower than the load effect, i.e., the limit state function (LSF) reaches zero or less. In the case of fatigue issue, the LSF can be established, as shown in Equation (7) [3,24,26].

$$g(D, t) = \Delta - D(t) \tag{7}$$

where  $\Delta$  is the damage tolerant factor, assumed as 1.0 in this study;  $D(t)$  stands for the time-dependent accumulation of fatigue damage.

The fatigue damage can be solved using the linear damage accumulation rule [37], as shown in Equation (8).

$$D(t) = \sum \frac{n_i(t)}{N_i} \tag{8}$$

where  $n_i(t)$  is the number of load cycles corresponding to stress range  $\Delta\sigma_i$ ;  $N_i$  is the allowable fatigue life under the stress range  $\Delta\sigma_i$ .

Through incorporating Equation (3), Equation (8) can be rewritten with an equivalent stress range  $\Delta\sigma_{re}$ , as shown in Equations (9) and (10).

$$D(t) = \Delta\sigma_{re}^m \cdot N(t) / C \tag{9}$$

$$\Delta\sigma_{re} = \sqrt[m]{\frac{\sum \Delta\sigma_i^m \cdot n_i(t)}{N(t)}} \tag{10}$$

where  $N(t)$  is the total number of loading cycles;  $C$  and  $m$  are the material-related constant and power index, respectively;  $\Delta\sigma_{re}$  is the equivalent stress range.

In the case of material properties, as aforementioned, the power index  $m$  is usually assumed as a deterministic value of 3 for welded joints in steel structure. Meanwhile, the constant  $C$  is assumed to follow the lognormal distribution, and the distribution parameters can be derived by the test data. According to [38], the damage tolerant factor  $\Delta$  follows the lognormal distribution, with the mean of 1 and coefficient of deviation (COV) of 0.3. The distribution parameters of the material properties are summarized in Table 3. It can be found from Table 3 that, although the COV of the constant  $C$  is smaller in TEU specimens than in CU specimens, the standard deviation of the fatigue strength is almost the same for the two types of specimens. This can be attributed to the improvement in the mean fatigue strength of TEUs specimen, i.e., more than 21% as previously illustrate in Table 2.

Table 3. Distribution of material properties.

Parameter	Type	CU Specimens		TEU Specimens	
		Nominal	Hot Spot	Nominal	Hot Spot
C	Mean ( $\times 10^{12}$ )	2.271	4.299	4.068	7.586
	COV	0.590	0.482	0.329	0.273
$\Delta$	Mean			1.0	
	COV			0.3	
$m$	Mean			3.0	

In the case of load effect, the total number of loading cycles  $N(t)$  can be regarded as a time-dependent deterministic value [39]. Meanwhile, the equivalent stress range can be solved using the in-situ measurement data, which will be discussed in detail in the following section.

Since the random variables related to the LSF of fatigue issue follows the normal or lognormal distribution, the analytic solution is available for the fatigue reliability  $\beta$ , as shown in Equations (11), (12) and (13).

$$\beta = \frac{(\lambda_C + \lambda_\Delta) - m \cdot \log(\Delta\sigma_{re}) - \log(N(t))}{\sqrt{\zeta_C^2 + \zeta_\Delta^2}} \tag{11}$$

$$\lambda_C = \log(\mu_C) - \log(1 + \delta_C^2)/2; \quad \zeta_C^2 = \log(1 + \delta_C^2) \tag{12}$$

$$\lambda_\Delta = \log(\mu_\Delta) - \log(1 + \delta_\Delta^2)/2; \quad \zeta_\Delta^2 = \log(1 + \delta_\Delta^2) \tag{13}$$

where  $\mu_C$  and  $\delta_C$  are the mean and COV of the material constant  $C$ ;  $\mu_\Delta$  and  $\delta_\Delta$  are the mean and COV of the damage tolerant factor  $\Delta$ .

#### 4.2. Derivation of Stress Spectra Using In-Situ Measurement

An OSD bridge in Chengdu, China was selected as the prototype for the further analysis of fatigue reliability. The prototype bridge consists of a 68 m-long main span and two 45 m-long side spans, which is a typical layout for urban steel bridges in China. The OSD system had been used in the bridge, carrying a fast lane, a middle lane and a slow lane. The sectional view of the prototype bridge is shown in Figure 10. Two critical details have been selected for the analysis, which are close to the frequent footprint of vehicles.

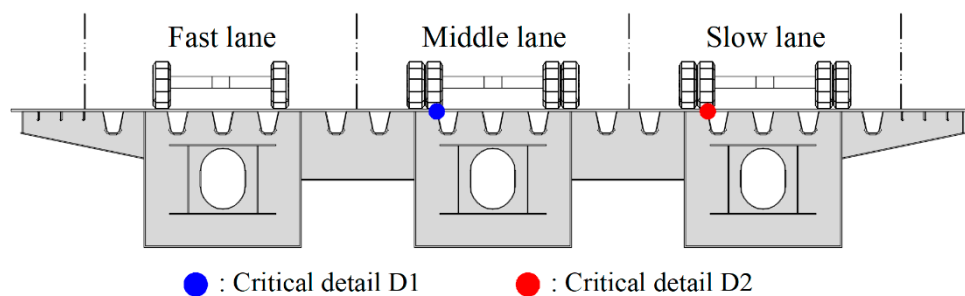


Figure 10. Sectional view of the prototype bridge.

In order to consider the uncertainty in vehicles passing through the bridge, the stochastic traffic model proposed in [27] was applied in deriving the stress spectra of the chosen details. The model consists of both the vehicle model including the vehicle-related properties and the lateral distribution of vehicles, which are described as random variables. Table 4 briefly illustrates the framework of the stochastic traffic model, and details could be found in [27].

Table 4. Illustration of the stochastic traffic model [27].

Model	Property	Description
Vehicle model	Axle number	The number of axles in a vehicle
	Axle spacing	The distance between the center of axles
	Axle weight	The weight of each axle in a vehicle
	Axle track	The distance between wheels in the same axle
	Footprint	The contact area of wheels on the deck
Lateral distribution	Occupancy rate	The distribution of the vehicle in different lanes
	In-lane position	The lateral position of the vehicle within a lane

In the vehicle model, the property is modelled by random variables using the in-situ measurement in [40,41]. According to the measurement, the vehicles can be divided into six different categories based on configuration, as briefly shown in Figure 11.



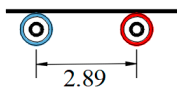
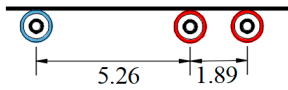
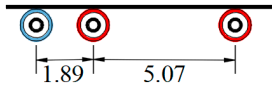
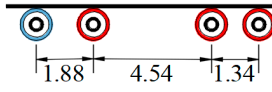
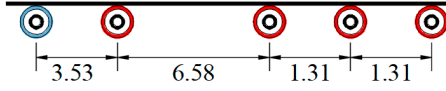
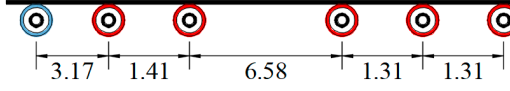
Type	Vehicle configuration (m)	Occupancy rate (%)		
		Fast	Middle	Slow
V1		41.23	25.74	9.70
V2		0.03	0.26	0.36
V3		0.10	0.87	0.60
V4		0.04	0.67	0.92
V5		0.06	1.17	1.31
V6		0.57	7.94	8.43

Figure 11. Vehicle category and occupancy rate [41].

Apart from the vehicle model, the occupancy rate in the lateral distribution can be also determined after the in-situ measurement shown in Figure 11. Besides, the distribution of the vehicle centre suggested in Eurocode 1 [42] has been used for the in-lane position.

A multi-scale finite element (FE) model of the prototype bridge was established using ANSYS software [43] to calculate the stress spectra of the chosen critical details, as shown in Figure 12. The FE model was established with the 3-dimensional shell element SHLL93 [44], including the global model of the entire bridge, the sub-model of the interested segment, and the local refined model of the critical details. In the global model, relatively coarse meshing was used to balance accuracy and efficiency since its task is to simulate the boundary condition of the interested segment. Compared with the global model, a much more refined meshing was applied to the sub-model, which serves as a transition between the coarse global model and the highly refined local meshing of the critical details. It is worth stating that the multi-point-constrain (MPC) method [45] was used to connect the global model and sub-model, through which the influence of difference on meshing size can be minimized. In the sub-model, the highly refined meshing (with the minimum size of 2 mm) was employed near the critical details to ensure the accuracy of stress results.

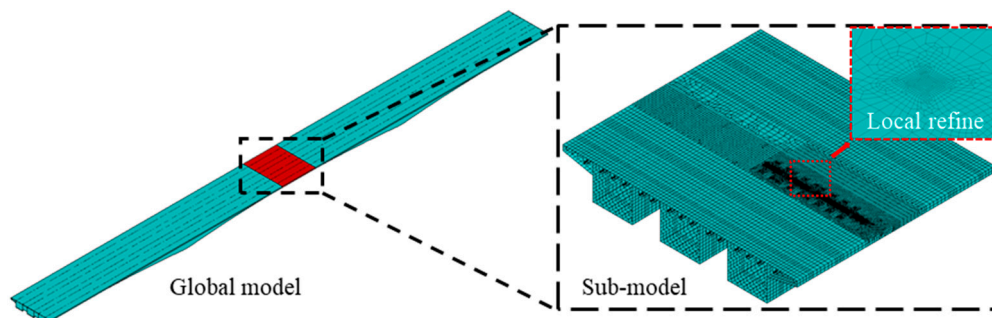


Figure 12. Multi-scale finite element model of the prototype bridge.

In the FE model, all the shell elements are arranged in the middle plane, as suggested by Hobbacher [36]. In solving the hot spot stress, the extrapolation method and reference points were kept the same as in the fatigue test, i.e., the “0515” rule. Since the local bending has influence mainly on the local nonlinear stress peak rather than the structural hot spot stress, the welds were not explicitly modelled. To this end, the reference points in the FE model were selected through their distance to the intersecting line between the deck plate and rib wall.

Based on the stochastic traffic model and multi-scale FE model, the in-situ measurement data was transferred into stress spectra, using the procedures illustrated in Figure 13.

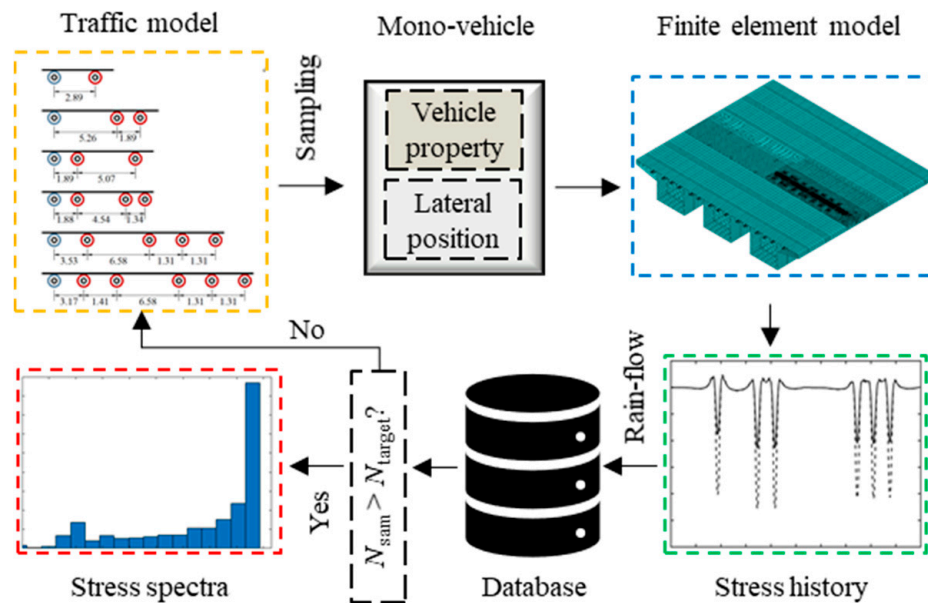


Figure 13. Procedures for stress spectra derivation.

The derivation is performed in a sampling-based way, in which the number of target samples is set as  $N_{target}$  (i.e.,  $10^6$  in this study). Through sampling with the measurement-based traffic model, information of the mono-vehicle can be generated. The information is then input to the FE model to calculate the stress history induced by the sampled vehicle, which is further processed to stress ranges using rain-flow cycle counting [46]. After that, the derived stress range is archived in a database and the above procedure will continue until the target number of samples is achieved. Finally, the stress spectra can be established through statistics on the derived database of stress ranges.

#### 4.3. Result and Discussion

Through the numerical approach illustrated in Section 4.2, the stress spectra of the two critical details were derived using in-situ measurement data. Figure 14a,b, respectively, shows the stress spectra of the two critical details D1 and D2 in terms of nominal stress. In both the spectra, the low-level stress range accounts for the largest portion. It is worth noting that the two details are in different lanes, while their stress spectra are highly similar. However, the similarity can be attributed to the almost same proportion of heavy trucks in the slow lane and middle lane. As shown in Figure 11, the occupancy rate is highly comparable in the two lanes for all the vehicle types except type V1, which represents lightweight vehicles. As generally acknowledged, lightweight vehicles have a very minor effect on the fatigue life of welded joints, even if their proportion are usually high in all the vehicles types. Meanwhile, after carefully checking the stress ranges from 5 to 30 MPa, it can be found that the stress ranges in the spectra of D2 are slightly higher than that of D1.

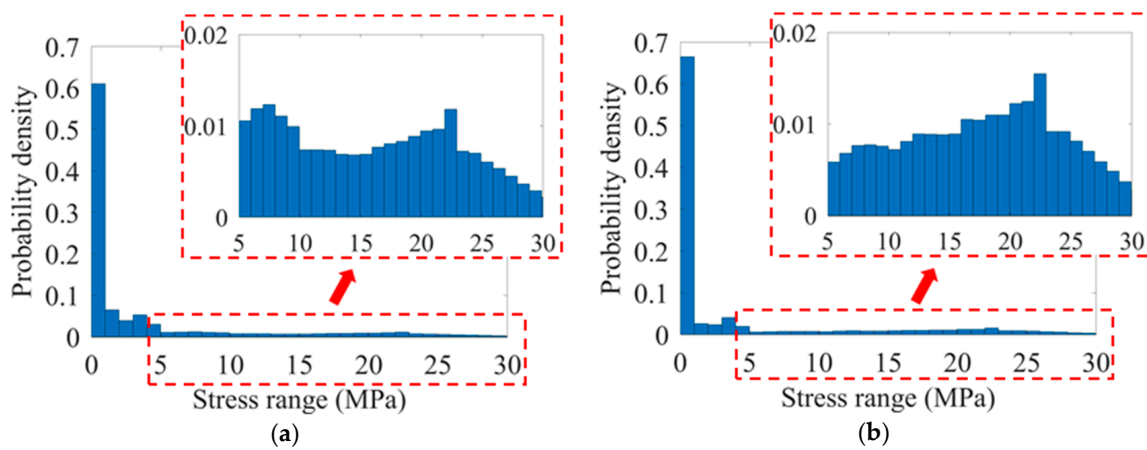


Figure 14. Stress spectra in terms of nominal stress: (a) critical detail D1 and (b) critical detail D2.

Also, the stress spectra of the two details were derived in terms of hot spot stress, as shown in Figure 15a,b.

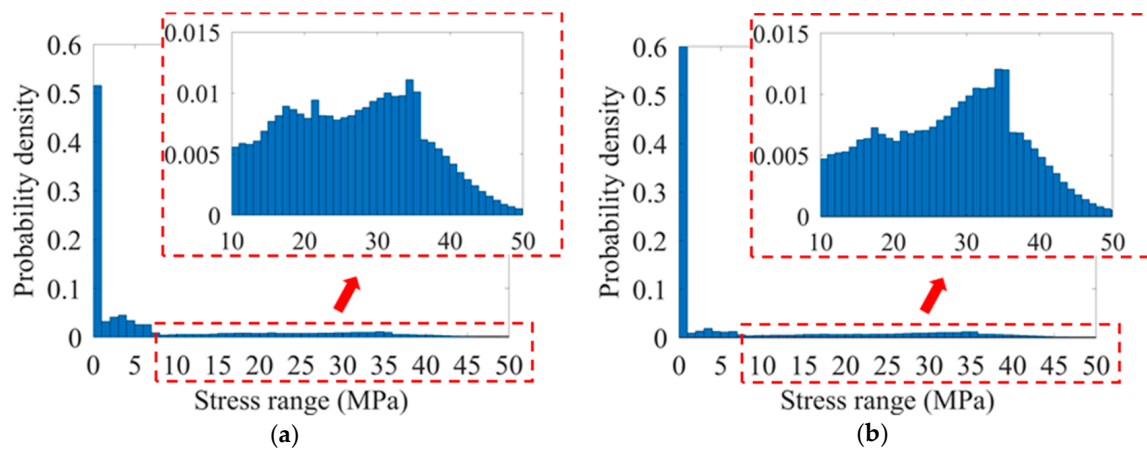
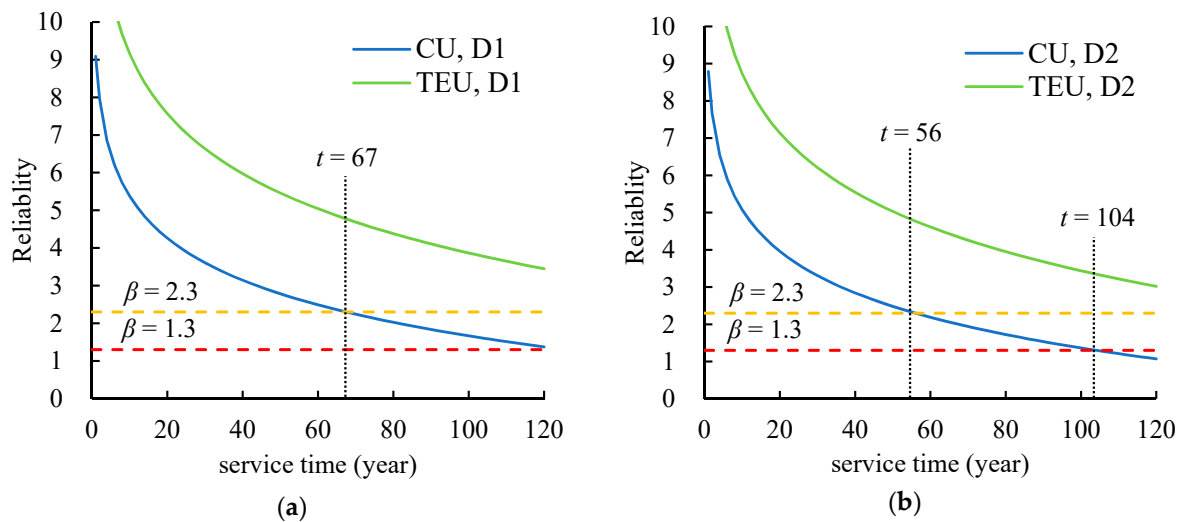


Figure 15. Stress spectra in terms of hot spot stress: (a) critical detail D1 and (b) critical detail D2.

Overall, the distribution and difference in the two types of spectra are almost the same as that in Figure 14a,b. However, the stress ranges in terms of hot spot stress are more continuous and even distributed than in terms of nominal stress. The result indicates that the hot spot stress-based spectra are able to reflect the randomness in vehicles more thoroughly than the nominal stress-based approach, through which a better accuracy can be expected for the prediction on fatigue life.

Through incorporating the above stress spectra into the calculation method in Section 4.1, the fatigue reliability of the two critical details can be solved. It is worth stating that the average daily traffic (ADT) is determined by the measurement data in [41], i.e., 5302 vehicles per direction per day. Besides, a design service life of 100 years is usually recommended for bridge structures [20,22]. However, for some vital structures such as the Hong Kong–Zhuhai–Macao bridge, an extended design life of 120 years can be applied [47]. To this end, the design lifespan of 120 years has been used in the reliability analysis. Based on the above analysis, the fatigue reliability can be solved for the two critical details in the OSD using CUs and OSD using TEUs. Figure 16a,b illustrates the reliability solved in terms of nominal stress, relating to the critical details D1 and D2, respectively.



**Figure 16.** Reliability in terms of nominal stress: (a) critical detail D1 and (b) critical detail D2.

As suggested by JCSS [48], the target reliability of 2.3 and 1.3 can be used for service limit checks when the efforts for enhancement are low and high, respectively. Thus, prediction can be made on the fatigue life using the two values above as the upper limit and lower limit of target reliability. It is worth stating that the target of 2.3 can be treated as a warning sign that inspection is required when the reliability is below 2.3, while the target of 1.3 can serve as a criterion for the fatigue life prediction. According to the result, in the OSD using CUs, the fatigue reliability of D1 reaches the upper limit after 67 years but stays above the lower limit up to the end. Meanwhile, the fatigue reliability of D2 reduces to the upper limit after 56 years and then the lower limit after 104 years. The result means that the design fatigue life of D2 is estimated as 104 years in terms of nominal stress. By contrast, in the OSD using TEUs, the fatigue reliability of both the two details is well above the upper limit line. The comparison suggests the fatigue life of rib-to-deck joints can be notably improved through the application of TEUs in OSDs.

The analysis has also been made in terms of hot spot stress, as shown in Figure 17a,b. In the OSD using CUs, the fatigue reliability of D1 reaches the upper limit after 43 years and then the lower limit after 74 years. A similar trend is shown in the reliability of D2 that the two limits are reduced to after 38 and 66 years, respectively. In the OSD using TEUs, the upper limit is reached in the details D1 and D2 after 109 and 97 years, respectively. However, the reliability of the two details stays well above the lower limit up to 120 years. The result in terms of hot spot also suggests an enhancement in fatigue life of RD joints by using TEUs. Meanwhile, it is worth noting that the reliability solved in hot spot stress is much lower than in nominal stress, indicating the conservativeness of the hot spot stress. Through considering the hot spot result with the lower limit, in the OSD using CUs, the design fatigue life can be predicted as 74 years for D1 and 66 years for D2. Under the same assumption, in the OSD using TEUs, the design fatigue life of D1 and that of D2 are well above 120 years. Besides, comparison can also be made based on the design fatigue life determined using the upper limit. As a result, the design fatigue life of D1 is 43 years in the OSD using CUs and 109 years in the OSD using TEUs, i.e., enhanced by about 153%. Similarly, for the detail D2, the design fatigue life is 38 years in the OSD using CUs while 97 years in the OSD using TEUs, i.e., about a 155% increment.



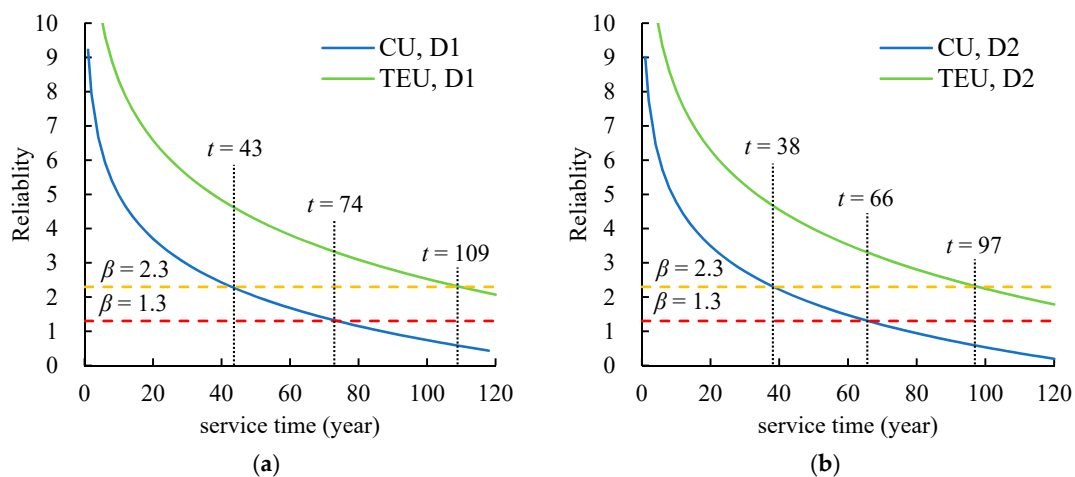


Figure 17. Reliability in terms of hot spot stress: (a) critical detail D1 and (b) critical detail D2.

## 5. Conclusions

In this paper, the fatigue performance of rib-to-deck (RD) joints in orthotropic steel decks (OSDs) was evaluated in a probabilistic way, using the fatigue test data and in-situ measurements. Two types of OSDs are investigated, including the OSD using conventional U-ribs (CUs) and the OSD using thickened edge U-ribs (TEUs). Fatigue tests were first carried out on the rib-to-deck specimens. Based on the test data of 18 specimens, the probability–stress–life (P–S–N) curve was derived for RD joints in the OSD using CUs and the OSD using TEUs, respectively. Then, an OSD bridge in China was selected as the prototype for further analysis. Through the stochastic traffic model, the in-situ measurement data was employed to derive the stress spectra of the critical RD joints, along with the multi-scale finite element (FE) model of the prototype bridge. After that, an analytic solution-based method was applied to calculate fatigue reliability of the critical joints based on the test data and derived stress spectra. Finally, comparisons have been made between the RD joint in the OSD using CUs and the one in the OSD using TEUs, in terms of the fatigue reliability.

According to the above analysis, the following conclusions can be drawn:

- (1) As per the fatigue test of rib-to-deck specimens, under the cyclic loading, the fatigue crack initiates at the deck toe and then propagates along the thickness and length of the deck plate until it penetrates through the deck plate and cause failure. The test result also proved the effectiveness of TEUs in enhancing the fatigue performance of RD joints. In the case of mean value, compared with the CU specimens, the fatigue strength of TEU specimens was 21.4% higher in nominal stress and 21.1% higher in hot spot stress.
- (2) Based on the test data of 18 specimens, P–S–N curves of RD joints were derived for the OSD using CUs and the OSD using TEUs, respectively. In the derivation, the statistics method proposed by IIW was employed after analysis, in which the survival rate of 95% is considered with the confidence of 75% for estimators. As a result, the FAT 90 and FAT 115 curves are suggested for the fatigue check of RD joints in the OSD using TEUs, in terms of nominal stress and hot spot stress, respectively. Meanwhile, for the RD joints in the OSD using CUs, the FAT 70 and FAT 90 curves are, respectively, recommended under the nominal stress and hot spot stress approaches.
- (3) A probabilistic framework was proposed to derive the stress spectra using the in-situ measurement data. In the derivation, a stochastic traffic model was applied to reflect the in-situ measurement of vehicles. Meanwhile, the multi-scale FE model of the selected prototype bridge was established to transfer the stochastic traffic into stress spectra. Through the large-scale sampling, the stress spectra of two critical RD joints were derived.
- (4) Based on the S–N approach, the limit state function of fatigue cracking was established. Then, investigations were then performed on the fatigue reliability of the two critical RD

joints selected, with the consideration of test data and in-situ measurements. The result indicated that the fatigue life of RD joints can be notably improved by using TEUs. For instance, under the target reliability of 2.3, the fatigue life of the two critical joints under the hot spot stress approach is increased by 153% and 155%, respectively. Meanwhile, the result also indicates the conservativeness of the hot spot stress approach over the nominal stress approach.

**Author Contributions:** Conceptualization, K.Z.; Data curation, Y.Z.; Funding acquisition, K.Z.; Methodology, J.H.; Supervision, K.Z.; Validation, J.H.; Writing—original draft, X.F.; Writing—review & editing, J.H. and J.Z.

**Funding:** The research was funded by the National Natural Science Foundation of China (grant number: 51778536), Doctoral Innovation Fund Program of Southwest Jiaotong University (grant number: D-CX201701), China Postdoctoral Science Foundation (grant number: 2019TQ9271), and Technology Foundation for Selected Oversea Chinese Scholar in Sichuan Province in 2019.

**Acknowledgments:** The corresponding author gratefully acknowledges financial support from China Scholarship Council and British Council during studying in the UK. Special thanks to Sakdirat at the University of Birmingham, and European Commission for H2020-MSCA-RISE Project No. 691135 “RISEN: Rail Infrastructure Systems Engineering Net-work” ([www.risen2rail.eu](http://www.risen2rail.eu)).

**Conflicts of Interest:** The authors declare no conflict of interest.

## References

- Connor, R.; Fisher, J.; Gatti, W.; Gopalaratnam, V.; Kozy, B.; Leshko, B.; Mc Quaid, D.L.; Medlock, R.; Mertz, D.; Murphy, T.; et al. *Manual for Design, Construction, and Maintenance of Orthotropic Steel Deck Bridges*; Federal Highway Administration: Washington, DC, USA, 2012.
- Wolchuk, R. Lessons from weld cracks in orthotropic decks on three European bridges. *J. Struct. Eng.* **1990**, *116*, 75–84. [[CrossRef](#)]
- Heng, J.; Zheng, K.; Kaewunruen, S.; Zhu, J.; Baniotopoulo, C. Dynamic Bayesian network-based system-level evaluation on fatigue reliability of orthotropic steel decks. *Eng. Fail. Anal.* **2019**, *105*, 1212–1228. [[CrossRef](#)]
- Fisher, J.W.; Roy, S. Fatigue of steel bridge infrastructure. *Struct. Infrastruct. Eng.* **2011**, *7*, 457–475. [[CrossRef](#)]
- Fisher, J.W.; Barsom, J.M. Evaluation of cracking in the rib-to-deck welds of the Bronx–Whitestone bridge. *J. Bridge Eng.* **2016**, *21*, 04015065. [[CrossRef](#)]
- Roy, S.; Mukherjee, S. *Design and Fabrication of Orthotropic Deck Details*; ATLSS Center, Lehigh University: Bethlehem, PA, USA, 2016.
- Wright, W. Orthotropic deck discussion group meeting. In Proceedings of the Orthotropic Bridge Design, Washington, DC, USA, 24 January 2011.
- Kolstein, M.H. *Fatigue Classification of Welded Joints in Orthotropic Steel Bridge Decks*; Delft University of Technology: Delft, The Netherlands, 2007.
- Haagensen, P.J.; Maddox, S.J. *IIW Recommendations on Methods for Improving the Fatigue Strength of Welded Joints: IIW-2142-110*; Woodhead Publishing: London, UK, 2013.
- Heng, J.; Zheng, K.; Gou, C.; Zhang, Y.; Bao, Y. Fatigue performance of rib-to-deck joints in orthotropic steel decks with thickened edge u-ribs. *J. Bridge Eng.* **2017**, *22*, 04017059. [[CrossRef](#)]
- Zhang, Q.; Li, J.; Yuan, D.; Bu, Y. Fatigue performance of rib-to-deck joint in orthotropic steel bridge deck with new type of both-side fillet welded joints. In Proceedings of the 40th IABSE Symposium, Nantes, France, 19–21 September 2018.
- Zhang, Q.; Liu, Y.; Bao, Y.; Jia, D.; Bu, Y.; Li, Q. Fatigue performance of orthotropic steel-concrete composite deck with large-size longitudinal U-shaped ribs. *Eng. Struct.* **2017**, *150*, 864–874. [[CrossRef](#)]
- Sim, H.B.; Uang, C.M.; Sikorsky, C. Effects of fabrication procedures on fatigue resistance of welded joints in steel orthotropic decks. *J. Bridge Eng.* **2009**, *14*, 366–373. [[CrossRef](#)]
- Ya, S.; Yamada, K.; Ishikawa, T. Fatigue evaluation of rib-to-deck welded joints of orthotropic steel bridge deck. *J. Bridge Eng.* **2011**, *16*, 492–499. [[CrossRef](#)]
- Meng, W.; Khayat, K.H.; Bao, Y. Flexural behaviors of fiber-reinforced polymer fabric reinforced ultra-high-performance concrete panels. *Cem. Concr. Compo.* **2018**, *93*, 43–53. [[CrossRef](#)]
- Liu, Y.; Zhang, Q.; Bao, Y.; Bu, Y. Static and fatigue push-out tests of short headed shear studs embedded in Engineered Cementitious Composites (ECC). *Eng. Struct.* **2019**, *182*, 29–38. [[CrossRef](#)]

17. Liu, Y.; Zhang, Q.; Meng, W.; Bao, Y.; Bu, Y. Transverse fatigue behaviour of steel-UHPC composite deck with large-size U-ribs. *Eng. Struct.* **2019**, *180*, 388–899. [[CrossRef](#)]
18. Heng, J.; Zheng, K.; Kaewunruen, S.; Zhu, J.; Baniotopoulos, C. Probabilistic fatigue assessment of rib-to-deck joints using thickened edge U-ribs. *Steel Compos. Struct.* **2020**, in press.
19. Heng, J.; Zheng, K.; Zhang, Y.; Wang, Y. Enhancing fatigue performance of rib-to-deck joints in orthotropic steel decks using thickened edge U-ribs. In Proceedings of the Structures Congress 2018, Fort Worth, TX, USA, 19–21 April 2018.
20. European Committee for Standardization (CEN). *BS EN 1993:2005 Eurocode 3: Design of Steel Structures*; CEN: Brussels, Belgium, 2005.
21. American Association of State Highway and Transportation Officials (AASHTO). *AASHTO LRFD Bridge Design Specifications*, 6th ed.; AASHTO: Washington, DC, USA, 2012.
22. Ministry of Transport of China (MOT). *JTG D64-2015 Specifications for Design of Highway Steel Bridge*; MOT: Beijing, China, 1 October 2015. (In Chinese)
23. Zhu, J.; Zhang, W. Probabilistic fatigue damage assessment of coastal slender bridges under coupled dynamic loads. *Eng. Struct.* **2018**, *166*, 274–285. [[CrossRef](#)]
24. Guo, T.; Frangopol, D.M.; Chen, Y. Fatigue reliability assessment of steel bridge details integrating weigh-in-motion data and probabilistic finite element analysis. *Comput. Struct.* **2012**, *112–113*, 245–257. [[CrossRef](#)]
25. Fan, L.; Bao, Y.; Meng, W.; Chen, G. In-situ monitoring of corrosion-induced expansion and mass loss of steel bar in steel fiber reinforced concrete using a distributed fiber optic sensor. *Compos. Part B-Eng.* **2019**, *165*, 679–689. [[CrossRef](#)]
26. Wu, M.; Zhu, J.; Heng, J.; Kaewunruen, S. Fatigue assessment on suspenders under stochastic wind and traffic loads based on in-situ monitoring data. *Appl. Sci.* **2019**, *9*, 3405. [[CrossRef](#)]
27. Heng, J.; Zheng, K.; Kaewunruen, S.; Baniotopoulos, C. Stochastic traffic-based fatigue life assessment of rib-to-deck welding joints in orthotropic steel decks with thickened edge U-ribs. *Appl. Sci.* **2019**, *9*, 2582. [[CrossRef](#)]
28. Tsakopoulos, P.A.; Fisher, J.W. Full-scale fatigue tests of steel orthotropic deck panel for the Bronx–Whitestone Bridge rehabilitation. *Bridge Struct.* **2005**, *1*, 55–66. [[CrossRef](#)]
29. Zeng, Z. Classification and reasons of typical fatigue cracks in orthotropic steel deck. *Steel Constr.* **2011**, *2*, 9–15. (In Chinese)
30. Kozy, B.; Connor, R. Fatigue Design of Orthotropic Steel Bridges. In Proceedings of the Structures Congress 2010, Orlando, FL, USA, 12–15 May 2010; pp. 541–550.
31. Standardization Administration of the People’s Republic of China (SAC). *GB/T 714-2008: Structural Steel for Bridge*; Standards Press of China: Beijing, China, 2008. (In Chinese)
32. Standardization Administration of the People’s Republic of China (SAC). *GB/T 10045-2001: Carbon Steel Flux Cored Electrodes for Arc Welding*; Standards Press of China: Beijing, China, 2001. (In Chinese)
33. American Welding Society (AWS). *AWS A5.20/A5.20M: 2005 Specification for Carbon Steel Electrodes for Flux Cored Arc Welding*; AWS: Miami, FL, USA, 2005.
34. MTS Systems Corporation. Mechanical Testing System; Eden Prairie, MN, USA. Available online: <https://www.mts.com/> (accessed on 1 October 2019).
35. Niemi, E.; Fricke, W.; Maddox, S.J. *Fatigue Analysis of Welded Components: Designer’s Guide to the Structural Hot-Spot Stress Approach*, 2nd ed.; Springer: Singapore, 2015.
36. Hobbacher, A. *Recommendations for Fatigue Design of Welded Joints and Components*, 2nd ed.; Springer: Berlin, Germany, 2015.
37. British Standards Institution (BSI). *BS 7910: 2013+A1:2015 Guide to Methods for Assessing the Acceptability of flaws in Metallic Structures*; BSI Standards Limited: London, UK, 2015.
38. Wirsching, P.; Chen, Y. Considerations of probability-based fatigue design for marine structures. *Mar. Struct.* **1988**, *1*, 23–45. [[CrossRef](#)]
39. Liu, Z.; Guo, T.; Chai, S. Probabilistic fatigue life prediction of bridge cables based on multiscale and mesoscopic fracture mechanics. *Appl. Sci.* **2016**, *6*, 99. [[CrossRef](#)]
40. Guo, T.; Liu, Z.; Zhu, J. Fatigue reliability assessment of orthotropic steel bridge decks based on probabilistic multi-scale finite element analysis. *Steel Constr.* **2015**, *11*, 334–346.

41. Guo, T.; Liu, Z.; Pan, S.; Pan, Z. Cracking of longitudinal diaphragms in long-span cable-stayed bridges. *J. Bridge Eng.* **2015**, *20*, 04015011. [[CrossRef](#)]
42. European Committee for Standardization (CEN). *BS EN 1991-2 Eurocode 1: Actions on Structure, Part 2: Traffic Load on Bridges*; CEN: Brussels, Belgium, 2003.
43. ANSYS Inc. *ANSYS Software*; ANSYS Inc.: Canonsburg, PA, USA; Available online: <https://www.ansys.com/> (accessed on 1 October 2019).
44. ANSYS Inc. *ANSYS Mechanical APDL Element Reference*; ANSYS Inc.: Canonsburg, PA, USA, 2018.
45. ANSYS Inc. *ANSYS Mechanical APDL Advanced Analysis Guide*; ANSYS Inc.: Canonsburg, PA, USA, 2018.
46. Amzallag, C.; Gerey, J.; Robert, J.; Bahuaud, J. Standardization of the rainflow counting method for fatigue analysis. *Int. J. Fatigue* **1994**, *16*, 287–293. [[CrossRef](#)]
47. Zhang, Q.; Cui, C.; Bu, Y.; Li, Q. Study on fatigue features of orthotropic decks in steel box girder of the Hong Kong-Zhuhai-Macao Bridge. *China Civil Eng. J.* **2014**, *47*, 110–119.
48. Joint Committee on Structural Safety (JCSS). *Probabilistic Model Code, Part 1: Basis of Design*; JCSS: Aalborg, Denmark, 2000.



© 2019 by the authors. Licensee MDPI, Basel, Switzerland. This article is an open access article distributed under the terms and conditions of the Creative Commons Attribution (CC BY) license (<http://creativecommons.org/licenses/by/4.0/>).